Continuously Changing the Conformational Dependence of Saponite Hybrid Materials on the Intercalation Degree: Electric Linear Dichroism of Stilbazolium Derivatives Intercalated in Saponite Clay

Ryo Sasai,# Tetsuya Shichi, Kunihiko Gekko,† and Katsuhiko Takagi*

Department of Crystalline Materials Science, Graduate School of Engineering, Nagoya University, Furuo-cho, Chikusa-ku, Nagoya 464-8603

†Department of Mathematical and Life Sciences, Graduate School of Science, Hiroshima University, Kagamiyama 1-3-1, Higashi-Hiroshima 739-8526

(Received March 2, 2000)

The molecular alignmet of 2- and 4-[4-(dimethylamino)styryl]-1-ethylpyridinium cations (2- and 4-DASEP, respectively) adsorbed on saponite clay and suspended in *N,N*-dimethylformamide (DMF) has been investigated by the electric linear dichroism (ELD) method. An ELD analysis of the saponite clay complex involving 4-DASEP molecules in DMF indicated that although the tilt angle of the 4-DASEP molecular plane increased considerably from 14.1 to 32.1°, the roll angle remained constant at ca. 31°, with a coverage of 10 to 100% of 4-DASEP molecular in saponite. In contrast, the tilt and roll angles of the corresponding positional isomer, 2-DASEP, on the clay surfaces slightly increased with the same coverage degrees. The change in tilt and roll angles in the 2- and 4-DASEP molecules may be significantly influenced by the structural variation of the guest molecules, especially the steric hindrance around the pyridinium N^+ atoms. The conformational structure of the adsorbed stilbazolium cations in saponite is discussed based on these results.

Clay minerals, i.e., negatively charged multilayered materials, possess a two-dimensional space, and various intercalated ionic or polar organic molecules are also able to exist in this space by ion-exchange reactions.[1—5] Moreover, the intercalated guest molecules have been found to gather as self-assembled aggregates due to hydrophobic interaction between them.[1—5] These unique and useful properties should open the way towards applications in promising functional devices in the field of materials science.[3,4]

Recently, clay minerals have attracted much attention as potential materials for the inorganic matrix of organic functional compounds.[3,4] The various organic guest molecules employed in these studies have been reported to naturally form functional self-assembled materials exhibiting such useful functions and properties as photochromism,[6—9] photochemical hole burning,[10—12] optical nonlinearity,[13,14] conductivity,[15] magnetism,[16,17] and stereoselective photochemical reactivity.[18—22] Although the self-assembly in clay interlayers has been investigated by various physicochemical methods,[23—26] a definite structure of the guest self-assembled aggregates has yet to be clarified in solvents.

In previous papers, we presented a detailed characterization of the structure of 4-chlorostilbene-4′-carboxylate (CSC) molecules in the layered double hydroxide (LDH) interlayers of *N,N*-dimethylformamide (DMF) by electric linear dichroism techniques.[27,28] Since the CSC molecules were found to self-assemble as a bilayer with a parallel orientation within the LDH interlayers in hybrid systems, the *syn* head-to-head dimers of the CSC molecules could be stereoselectivity produced by UV irradiation.

In this paper, two positionally isomeric stilbazolium cations (2- and 4-DASEP) were investigated not only to see the structural effect of the guests on the aggregated conformations, but also in order to develop photofunctional devices, which would possess a high hyperpolarizability and exhibit nonlinear optical properties, such as second-harmonic generation. To this end, the electric linear dichroism analysis can be considered to be an intriguing method to establish the exact orientation and detailed conformation of the self-assembled structure formed on the synthetic saponite clay surface. At the same time, the tilt and roll angles of the self-assembled hybrid materials formed were found to be easily controlled by changing the amount of the intercalated guest molecules and varying the positions of the cationic sites within the guest molecules.

Experimental

The UV-visible spectra were recorded on a JASCO V-550 UV-vis spectrophotometer at room temperature.

Materials. The 4-[4-(dimethylamino)styryl]-1-ethyl-

Present address: Research Center for Advanced Waste and Emission Management, Nagoya University, Furuo-cho, Chikusa-ku, Nagoya 464-8603.

pyridinium iodide (4-DASEP) was obtained from Nippon Kankoh Shikiso Kenkyusho (Okayama) and used without further purification. The 2-[4-(dimethylamino)styryl]-1-ethylpyridinium iodide (2-DASEP) was purchased from Aldrich Chemical Co., Inc., and used without further purification. Scheme 1 shows the structural formula of these compounds. It is well known that these stilbazolium derivatives exhibit a second-harmonic generation phenomenon in the anti-centresymmetric single crystal. The synthetic saponite clay mineral, Sumecton SA (SA), was provided by Kunimine Ind., Ltd., Japan, the chemical formula of which is $(Na_{0.49}Mg_{0.14})^{0.77+}[(Si_{7.20}Al_{0.80})(Mg_{5.97}Al_{0.03})O_{20}(OH)_4]^{0.77-}$. The cation-exchange capacity (CEC) of the SA was estimated to be ca. 1.0 mequiv/g.

Preparations. One gram of the SA powder was dispersed in 500 mL of distilled and ion-exchanged water by sonication. The appropriate quantity of each stilbazolium derivative was added as a powder to this SA suspension under magnetic stirring at room temperature. To complete the intercalation of the DASEP molecules within the SA interlayers, the resulting suspended mixture was heated and kept one more night at 60 °C. The resulting light or reddish precipitate was passed through a membrane filter (pore size 0.20 μm) and dried overnight in vacuo at room temperature. The molar ratios of the added DASEP molecules to the CEC of the SA clay, [DASEP]/[SA], were adjusted at 0.1, 0.5, and 1.0.

Ten milligrams of SA clay with the intercalated DASEP molecules were dispersed in 10 mL of DMF by sonication. After the large aggregated particles in the dispersion were removed by centrifugation at 2000 rpm for 10 min at room temperature, the supernatant was analyzed by the electric linear dichroism (ELD) techniques. The homogeneity of the dispersed hybrid particles in this supernatant was confirmed to monitor the front-light-scattering intensity at 700 nm. An ELD analysis was carried out at room temperature in the range 300—600 nm with an electric-field strength of $E \leq$ ca. 25 kVcm^{-1} on a self-made apparatus which is able to separately detect both parallel ($\Delta A_{\parallel}$) and perpendicular ($\Delta A_{\perp}$) dichroism signals. The details of this ELD apparatus have been described in previous literature.[27—30]

The reduced electric linear dichroism ($\Delta A/A$) of the chromophores in suspension can be defined as

$$\Delta A/A = (A_{\parallel} - A_{\perp})/A = 1.5 \times (3\cos^2\theta - 1) \bullet \Phi(E) = (\Delta A/A)_s \bullet \Phi(E), \quad (1)$$

where A is the absorbance in the absence of an electric field; θ is the angle between the direction of the optical transition moment of the chromophore and orientation axis, which should coincide with the normal line of the clay surface in the present study; $(\Delta A/A)_s$ is the saturated or intrinsic reduced dichroism at infinitely high field strength; and $\Phi(E)$ is the orientation function of the clay particles at a given field strength, E, which is independence of the wavelength. Since the shape of a clay particle is assumed to be a platelet, the value of $\Phi(E)$ becomes -0.5 at infinitely higher field strengths.[31,32]

Since a guest molecule may be excited by a series of electronic transitions, the observed absorption spectrum is composed of a sum of a series of these partial bands. Thus, the observed wavelength dependence of the saturated reduced dichroism, i.e., ELD spectrum, is composed of these partial bands obtained by deconvolution of the guest molecules adsorbed regularly on the clay surface and by an estimation on the basis of computer-assisted iteration procedures. Details of the ELD spectrum analyses have also been described in previous papers.[27,28,33]

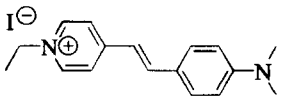

4-[4-(dimetylamino)styryl]-1-ethylpyridinium iodide (4-DASEP)

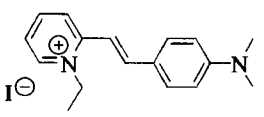

2-[4-(dimetylamino)styryl]-1-ethylpyridinium iodide (2-DASEP)

Scheme 1. Structural formula of the DASEP compounds.

Results and Discussion

UV-Visible Absorption Spectra of DASEP. Figure 1 shows the UV-visible absorption spectra of the DASEP molecules, (a) 4- and (b) 2-DASEP, in the absence and the presence of SA clay in DMF. The absorption spectra of the DASEP molecules without SA clay (solid line) show an absorption maximum at 470 nm (4-DASEP) and at 463 nm (2-DASEP), respectively. The wavelength of the absorption maximum shifted slightly to shorter wavelengths on the SA

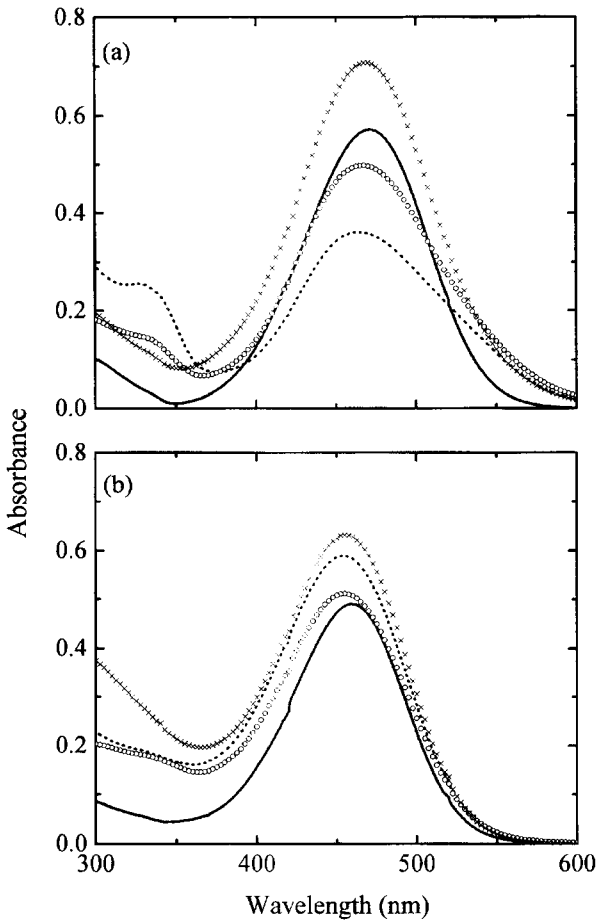

Fig. 1. UV-visible absorption spectra of DASEP molecules in the absence and presence of SA clay minerals in DMF: (a) 4-DASEP and (b) 2-DASEP. Solid lines indicate the spectrum in the absence of the SA clay minerals. [DASEP]/[SA] = 0.1 (dotted lines), 0.5 (circles), and 1.0 (crossed hair).

clay surface, with an additional absorption, which newly appeared at around 330 nm when incorporated in the SA clay. These blue shiftsts in the adsorption maximum could be assumed to be due to a change of the more hydrophobic nature along with an increase of the adsorption degree, though not decisive.

ELD Spectra of DASEP–SA Hybrid Materials. Figure 2 shows the ELD spectra of the DASEP–SA hybrid materials suspended in DMF. The ELD spectra of the 4-DASEP–SA hybrid materials show their profile with increasing the coverage degree of the 4-DASEP in SA ([4-DASEP]/[SA] = 0.1, 0.5, and 1.0), as shown in Fig. 2a. The spectra were not constant, but were dependent on the wavelength within the 300—600 nm range, exhibiting a maximum in the 300—350 nm region and with a shoulder at around 420—480 nm. The $(\Delta A/A)_s$ values depended on the [4-DASEP]/[SA] ratios only in the 420—480 nm region. In this region, the 4-DASEP molecule possesses an optical transition moment along the long-molecular axis. Hence, these results indicate that the inclination of the 4-DASEP molecular plane against the clay surface changes with an increase in the degree of coverage of the intercalated 4-DASEP. On the other hand, the profile of the ELD spectrum of each 2-DASEP–SA hybrid material did not change with an increase in the [2-DASEP]/[SA] ratios, although the level ELD spectra of the 2-DASEP–SA hybrid materials could not be observed. The $(\Delta A/A)_s$ values between 420—480 nm indicate that the tilt angle of the 2-DASEP molecular plane against the clay surface actually shows no change upon varying the coverage of 2-DASEP on the layer surface of the SA clay. This wavelength dependency led to the conclusion that the observed ELD spectrum consists of number of absorption bands of the DASEP molecule. The deconvolution of the isotropic absorption spectrum into partial bands and the determination of the direction for the optical transition dipole moments of these bands are important for a quantitative discussion of the conformation of the DASEP molecules absorbed in the SA clay interlayers.

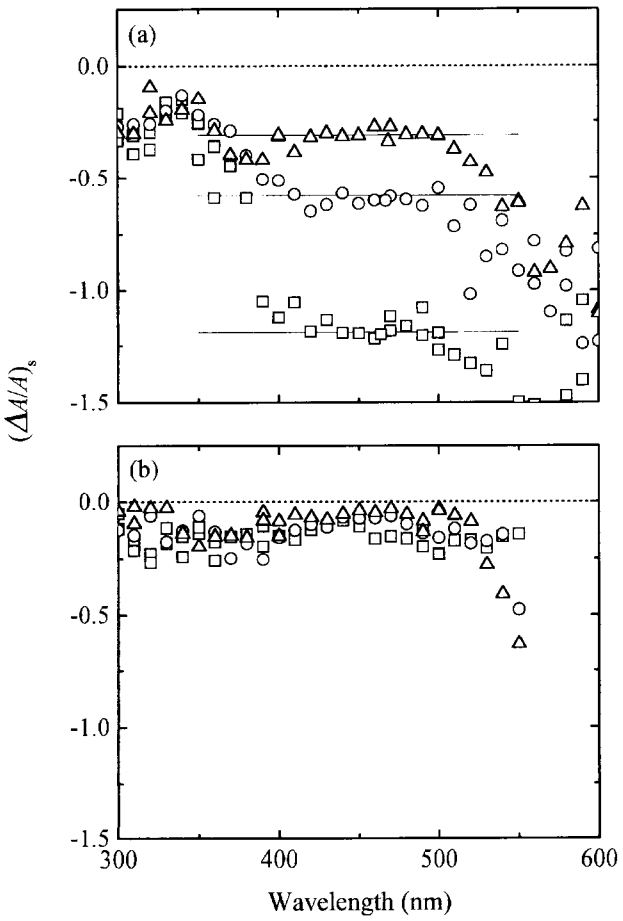

Fig. 2. ELD spectra of DASEP–SA hybrid materials suspended in DMF: (a) 4-DASEP and (b) 2-DASEP. [DASEP]/[SA] = 0.1 (squares), 0.5 (circles), and 1.0 (triangles).

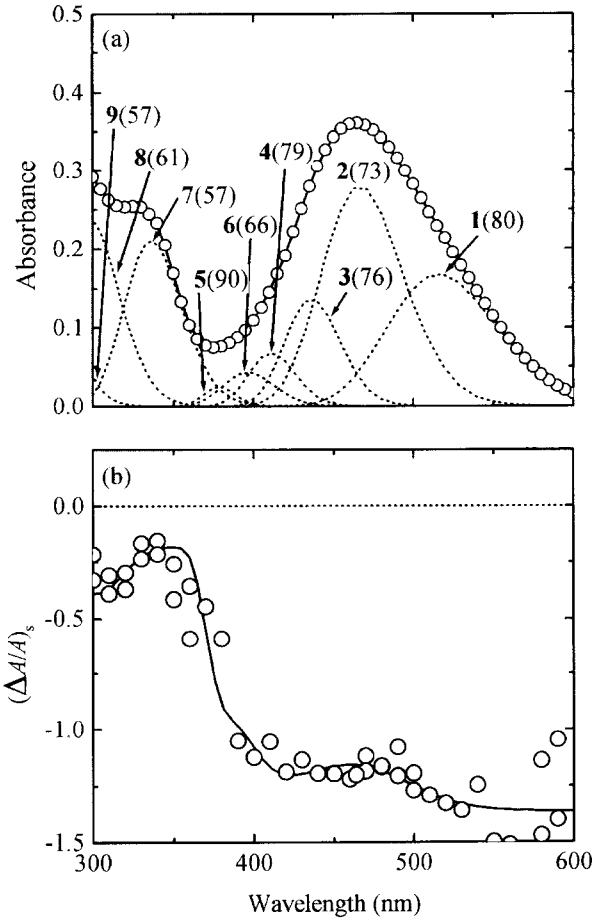

Fig. 3. (a) Deconvolution of the observed isotropic absorption spectrum of 4-DASEP and (b) fitting of the corresponding ELD spectrum in the presence of the SA clay at [4-DASEP]/[SA] = 0.1. The partial absorption bands (broken lines) involved in the isotropic spectrum were numbered from the longer wavelengths from 1 to 9. The resulting spectrum from these partial bands is shown with a solid line. The figure for each partial absorption band means the angle of θ, with which the ELD spectrum was reproduced in figure (b) (solid line), although the experimental isotropic and ELD spectra were continuous, with respect to the wavelength.

Deconvolution of the Isotropic Absorption Spectra and Simulation of the ELD Spectra of DASEP. In an observation of the absorption spectrum of DASEP molecules, Figs. 3 and 4 show the deconvolution into partial bands (broken lines in Figs. 3b and 4b with [DASEP]/[SA] = 0.1, without applying an electric field. An excellent agreement between the observed (circles) and calculated (solid line) values can be found in the observed ELD spectrum, which was simulated (Figs. 3a and 4a) by giving the appropriate value of angle θ to each partial band of the DASEP molecule. Applying this procedure to the observation data, all of the observed absorption spectra could be deconvoluted into partial bands, and all of the measured ELD spectra could be exactly represented by providing an appropriate value of angle θ to each partial band.

Estimation of the Direction of the Optical Transition Moments in the DASEP Plane and their Assignment to the Partial Bands. In order to calculate the roll and tilt angles of the DASEP molecules, angle ξ between the roll axis (y axis in Fig. 5) of DASEP and the direction of the optical transition dipole moment for each DASEP molecule is necessary. Since no data for the transition moments are available for the DASEP molecules adsorbed in the SA clay, angle ξ was estimated by MO calculations.[34] The calculation for a single DASEP molecule by the ZINDO/S method was performed according to the following procedures: (1) The molecular structure of DASEP was optimized by the PM3 method;[35] (2) the electronic states of this optimized structure were then calculated by the ZINDO/S method; (3) the position and direction of each optical transition moment was estimated.

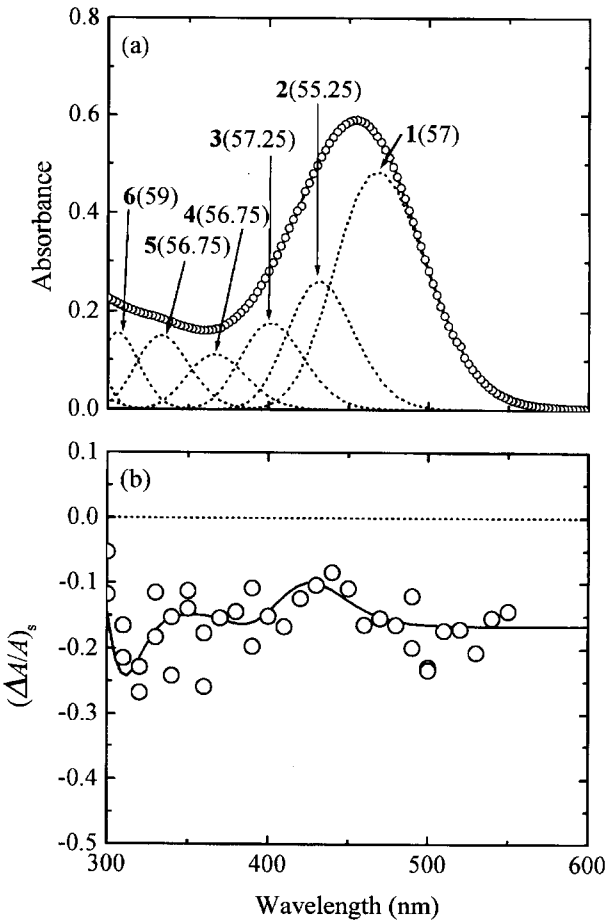

Fig. 4. (a) Deconvolution of observed isotropic absorption spectrum of 2-DASEP and (b) fitting of the corresponding ELD spectrum in the presence of SA clay at [2-DASEP]/[SA] = 0.1. The partial absorption bands (broken lines) involved in the isotropic spectrum were numbered from the longer wavelength side from 1 to 6. Other notations and symbols are the same as those in Fig. 3.

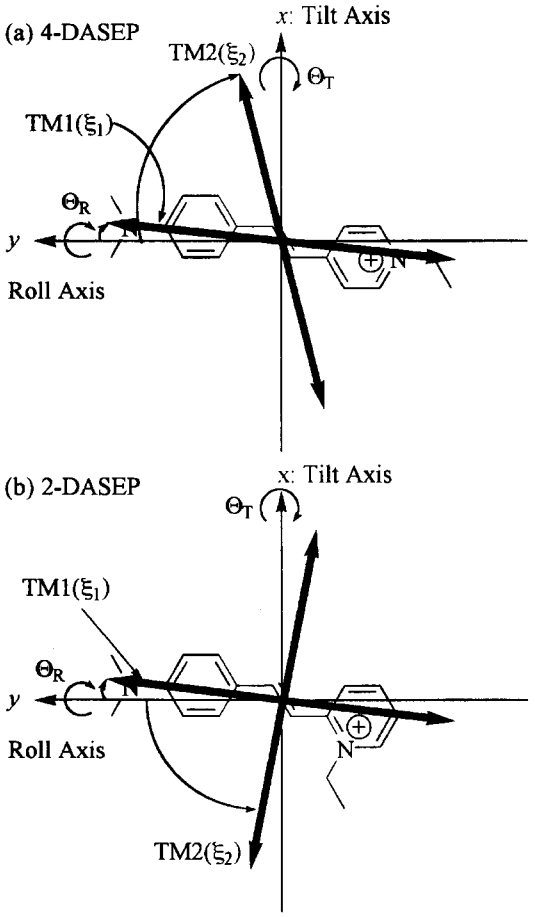

Fig. 5. Direction of the optical transition moments of 4- and 2-DASEP molecules calculated by the ZINDO/S method.

Figure 5 shows both the direction of the optical transition moments and angle ξ calculated by ZINDO/S within the (a) 4-DASEP and (b) 2-DASEP molecular planes. These calculations provide important information on the direction of the optical transition moment, as follows: (1) The DASEP molecule possesses two main optical transition moments in the DASEP plane. One is transition moment 1 (TM1) in which $\xi = 5.8°$ (4-DASEP) and 6.3° (2-DASEP) and which is almost parallel to the long-molecular axis, while the other is transition moment 2 (TM2) in which $\xi = 75.6°$ (4-DASEP) and $\xi = -79°$ (2-DASEP); (2) TMI is responsible for the absorption in the long-wavelength region; (3) the absorption in the short-wavelength region is caused by the optical TM2. These estimations need to be assigned to the partial bands,

Table 1. Optical Transition Dipole Moment Calculated by ZINDO/S and the Assignment to Each Partial Band

DASEP	Transition moment	$\lambda_{ZINDO/S}$ [a] nm	ξ_j deg	λ_{obs} [b](θ_j [c])/nm (deg) 0.1 [d]	0.5 [d]	1.0 [d]
4-DASEP	TM1	422.6	5.8	467 (73)	465 (61)	485 (55)
	TM2	280.9	75.6	336 (57)	339 (57)	332 (56)
2-DASEP	TM1	422.7	6.3	468 (57)	465 (56)	465 (56)
	TM2	256.3	−79.0	306 (59)	310 (57)	310 (55)

a) This wavelength was calculated for the single DASEP molecle by the ZINDO/S method in vacuo.
b) This wavelength was estimated from the deconvolution of the observed isotropic absorption spectra.
c) This value was estimated from the best-fitting ELD simulated by using partial absorption bands.
d) These values are the [DASEP]/[SA] ratios.

because they do not reflect the actual moments in the clay. The deconvolution of the absorption spectrum of the DASEP molecules without the SA clay was used for the assignments using the data given in Table 1.

Evaluation of Roll Θ_R and Tilt Θ_T Angles. The roll Θ_R and the tilt Θ_T angles for the DASEP molecule within the SA clay interlayers can be evaluated with the obtained ξ values, respectively, as shown in Fig. 5. Angles Θ_R and Θ_T are expressed by using angle θ_j for the jth partial band and angle ξ_j for the jth transition moment by employing

$$\cos\theta_j = -\cos\Theta_T\sin\Theta_R\sin\xi_j + \sin\Theta_T\cos\xi_j, \quad (2)$$

where the signs of Θ_R and Θ_T are taken to be positive for a clockwise rotation, which is viewed from the negative-to-positive directions of the x and y axis, as shown in Fig. 5.

Table 2 shows the roll angle, Θ_R, and the tilt angle, Θ_T, for all [DASEP]/[SA] ratios calculated from Eq. 2. It should be noted that there are considerable differences in the dependence of the loading amounts of DASEP upon Θ_R and Θ_T between the 2- and 4-isomers of the molecules. In the case of the 4-DASEP–SA hybrid materials, the tilt angle, Θ_T, of the adsorbed 4-DASEP molecules increase from 14.1 to 32.1° along with an increase in the [4-DASEP]/[SA] ratios, while the roll angle, Θ_R, remains almost constant at around 31°, even when the ratio increases from 0.1 to 1.0. Such an increase in the tilt angle is conceivable on the assumption that 4-DASEP can interact with the anionic sites of the clay surface at the terminal pyridinium nitrogen atom of 4-DASEP; this is called "head-on type" adsorption, as shown in Fig. 6. At low loadings, 4-DASEP lies almost flat on the layer surface and occupies a rather large area on the surface (Fig. 6a). However, with an increase in the [DASEP]/[SA] ratios, the layer surface becomes covered and crowded by the DASEP and can no longer accommodate all of the guest molecules (Figs. 6b and 6c). In spite of these restrictions, however, as the added guests continue to interact with the surface anionic sites by means of electrostatic interactions, they tend to stand with a certain tilt. In fact, the results of an XRD analysis (Table 3) shows that the clay powder sample possesses basal spacings, $^{dry}d_{001}$, which can be steadily increased with a higher coverage of 4-DASEP. The estimated increase in the tilt angles of 4-DASEP can be well understood on the basis of the above phenomenon.

Table 3 also includes figures of the basal spacings, $^{wet}d_{001}$, of the clays intercalated by 4-DASEP and soaked in DMF. In the case of the DMF-soaked clay sample, however, the basal spacing was almost constant or, unexpectedly, smaller with high loadings. This observation suggests an important point that DMF may penetrate into the interlayer space of the 4-DASEP included clay minerals, and opening a space wider than in the case of 4-DASEP alone. The ELD analysis carried out in this investigation was able to clarify the detailed alignments of the guest molecular packing in solvent-suspended clay, which was not possible with an XRD analysis alone.

In contrast to 4-DASEP, the corresponding 2-isomer is subject to a more complicated change along with an increase in the loading amounts of the guest molecules. That is,

Table 2. Angles Θ_R and Θ_T of DASEP Molecules Adsorbed to SA Clay Surface Evaluated from ELD Analysis[a]

DASEP	[DASEP]/[SA]	Θ_R deg	Θ_T deg
4-DASEP	0.1	31.0	14.1
	0.5	30.0	26.2
	1.0	31.4	32.1
2-DASEP	0.1	24.1	36.6
	0.5	26.2	38.3
	1.0	27.5	38.9

a) Errors of all angle data are±0.5°.

Table 3. Basal Spacings, d Estimated from X-Ray Diffraction Analysis

DASEP	[DASEP]/[SA]	$^{dry}d_{001}$ nm	^{wet}d [a] nm
4-DASEP	0.1	1.45	2.29
	0.5	1.55	1.65
	1.0	1.60	1.69
2-DASEP	0.1	1.41	2.22
	0.5	1.57	2.26
	1.0	1.63	2.13

a) Soaked by *N*,*N*-dimethylformamide.

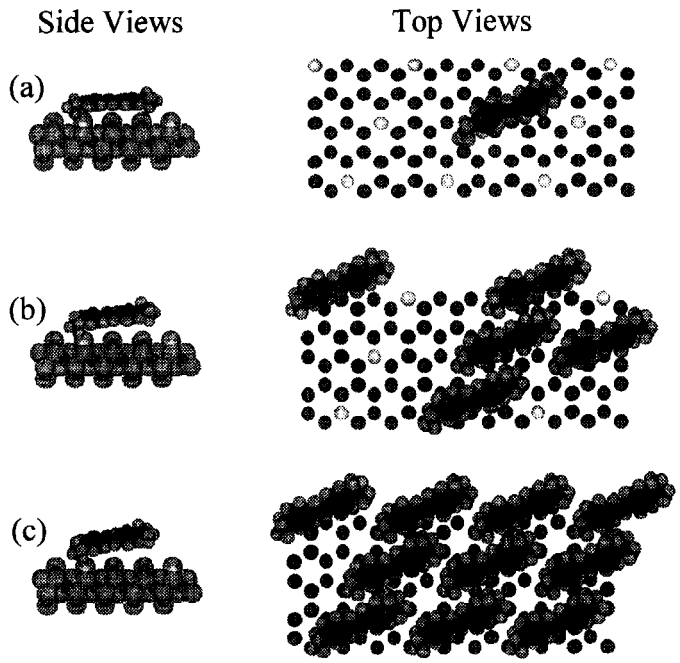

Fig. 6. Adsorption models of 4-DASEP molecules on the clay surfaces. [DASEP]/[SA]; (a) 0.1 (b) 0.5, and (c) 1.0.

not only the tilt angle, Θ_T, but also the roll angle, Θ_R, increase with an increase in the amounts of the loaded 2-DASEP, given in Table 2. This loading dependency of the angle may be attributed to a structural effect of the DASEP molecules. 2-DASEP interacts with the anionic sites of the interlayer surface at its 2-position substituted by a cationic nitrogen atom, which is located at an unsymmetrical position of the molecule, which is called "edge-on type" adsorption, as shown in Fig. 7. When 2-DASEP stands up from the surface by the loading of increasing amounts of 2-DASEP without changing the roll angle, the cationic nitrogen moves apart from the anionic sites, inducing a thermodynamically unfavorable movement. In order to compensate the instability, it seems more favorable if the 2-DASEP molecule not only tilts, but also rolls not far from the anionic sites of the layer surface. This is not the case of 4-DASEP, which is a symmetrical molecule having a cationically charged nitrogen atom at the terminal position of 4-DASEP.

Conclusions

In the present study, the orientation behavior of two isomeric DASEP, i.e., 2- and 4-DASEP, adsorbed on the SA clay surface at various [DASEP]/[SA] ratios was determined by using an ELD analysis. Both DASEP molecules were found to form closely pocked self-assemblies on the clay surface in which both show a different inclination, depending on the loading degrees. The roll angle of 4-DASEP, but not the tilt angle, remains constant. In contrast, 2-DASEP varies in both the tilt and roll angles along with an increase in the amounts of the intercalated 2-DASEP. These observation are rational based on the assumption that a symmetrical 4-isomer need not roll, but an unsymmetrical 2-isomer must roll in order to maintain a close interaction between the cationic nitrogen and the anionic site.

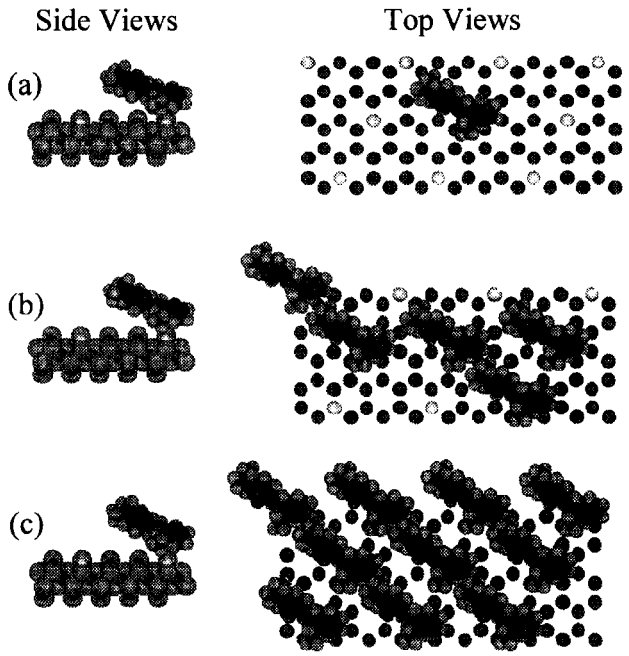

Fig. 7. Adsorption models of 2-DASEP molecules on the clay surfaces. [DASEP]/[SA]; (a) 0.1, (b) 0.5, and (c) 1.0.

We would like to thank Mr. Jyun-ichi Itoh of Kunimine Ind., Ltd., for kindly donating the synthesized saponite clay, Sumecton SA, and also providing characterization data. This work was supported in part by a Grant-in-Aid Fund from the Ministry of Education, Science, Sports and Culture.

References

1 R. E. Grim, "Clay Mineralogy," McGraw-Hill, New York (1953).

2 Kikan Kagaku Sosetsu No. 4, "Chemistry of Soils," ed by the Chemical Society of Japan, Japan Scientific Societies Press, Tokyo (1994).

3 Kikan Kagaku Sosetsu No. 21, "Microporous Crystals," ed by the Chemical Society of Japan, Japan Scientific Societies Press, Tokyo (1994).

4 Kikan Kagaku Sosetsu No. 36, "Fundamental and Advances in Photochemistry," ed by the Chemical Society of Japan, Japan Scientific Societies Press, Tokyo (1998).

5 M. S. Whittingham and A. J. Jacobson, "Intercalation Chemistry," Academic Press, New York (1982).

6 K. Takagi, T. Kurematsu, and Y. Sawaki, *J. Chem. Soc., Perkin Trans. 2*, **1991**, 1517.

7 M. Ogawa, K. Fujii, K. Kuroda, and C. Kato, *Mater. Res. Soc. Symp. Proc.*, **233**, 89 (1991).

8 M. Ogawa and A. Ishikawa, *J. Mater. Chem.*, **8**, 463 (1998).

9 T. Seki and K. Ichimura, *Macromolecules*, **23**, 31 (1990).

10 M. Ogawa, M. Takahashi, C. Kato, and K. Kuroda, *J. Mater. Chem.*, **4**, 519 (1994).

11 M. Ogawa, T. Hnada, K. Kuroda, C. Kato, and T. Tani, *J. Phys. Chem.*, **96**, 8116 (1992).

12 K. Sakoda and K. Kiminami, *Chem Phys. Lett.*, **216**, 270 (1993).

13 S. Cooper and P. K. Dutta, *J. Phys. Chem.*, **94**, 114 (1990).

14 M. Ogawa, M. Takahashi, and K. Kuroda, *Chem. Mater.*, **6**, 715 (1994).

15 E. Ruiz-Hitzky, *Adv. Mater.*, **5**, 334 (1993).

16 L. V. Govea and H. Stenfink, *Chem. Mater.*, **9**, 849 (1997).

17 W. Fujita and K. Awaga, *J. Am. Chem. Soc.*, **119**, 4563 (1997).

18 a) K. Takagi, H. Usami, H. Fukaya, and Y. Sawaki, *J. Chem. Soc., Chem. Commun.*, **1989**, 1174. b) H. Usami, K. Takagi, and Y. Sawaki, *J. Chem. Soc., Perkin Trans. 2*, **1990**, 1723.

19 H. Usami, K. Takagi, and Y. Sawaki, *J. Chem. Soc., Faraday Trans.*, **88**, 77 (1992).

20 K. Takagi, T. Shichi, H. Usami, and Y. Sawaki, *J. Am. Chem. Soc.*, **115**, 4339 (1993).

21 T. Shichi, K. Takagi, and Y. Sawaki, *Chem. Commun.*, **1996**, 2027.

22 T. Shichi, K. Takagi, and Y. Sawaki, *Chem. Lett.*, **1996**, 781.

23 S. Yamanaka, F. Kanamaru, and M. Koizumi, *J. Phys. Chem.*, **79**, 1285 (1975).

24 M. Raupach, W. W. Emerson, and P. G. Slade, *J. Colloid Interface Sci.*, **69**, 398 (1979).

25 M. B. McBride, *Clays Clay Miner.*, **33**, 510 (1985).

26 C. Breen, J. M. Adams, and C. Rieckel, *Clays Clay Miner.*, **33**, 275 (1985).

27 R. Sasai and K. Takagi, *New Ceram.*, **11**, 40 (1998).

28 R. Sasai, T. Shin'ya, T. Shichi, K. Takagi, and K. Gekko, *Langmuir*, **15**, 413 (1999).

29 K. Yamaoka and K. Matsuda, *Macromolecules*, **14**, 595 (1981).

30 K. Yamaoka, Y. Yamamoto, Y. Fujita, and N. Ojima, *J. Phys. Chem. B*, **101**, 837 (1997).

31 R. Sasai and K. Yamaoka, *J. Phys. Chem.*, **99**, 17754 (1995).

32 R. Sasai, N. Ikuta, and K. Yamaoka, *J. Phys. Chem.*, **100**, 17266 (1996).

33 N. Ojima, K. Fukudome, and K. Yamaoka, *J. Sci. Hiroshima Univ., Ser. A*, **59**, 119 (1995).

34 a) J. E. Ripley and M. C. Zerner, *Theoret. Chim. Acta*, **32**, 111 (1973). b) A. D. Bacon and M. C. Zener, *Theoret. Chim. Acta*, **53**, 21 (1979). c) M. C. Zerner, G. H. Loew, R. F. Krichener, and U. T. Mueller-Westerhoff, *J. Am. Chem. Soc.*, **102**, 589 (1980). d) "ZINDO Reference Manual," Cache Science Corporation, Beanerton, Oregon (1993). e) M. Adachi and S. Nakamura, *Dyes Pigm.*, **17**, 287 (1991).

35 J. J. P. Stewart, *J. Comput. Chem.*, **10**, 209 (1989).